



Universidade de São Paulo

Biblioteca Digital da Produção Intelectual - BDPI

Departamento de Física e Ciências Materiais - IFSC/FCM

Artigos e Materiais de Revistas Científicas - IFSC/FCM

2009-03

Intense blue and green photoluminescence emissions at room temperature in barium zirconate powders

Journal of Alloys and Compounds, Lausanne, v. 471, n. 1/2, p. 253-258, Mar. 2009

<http://www.producao.usp.br/handle/BDPI/49334>

Downloaded from: Biblioteca Digital da Produção Intelectual - BDPI, Universidade de São Paulo



Intense blue and green photoluminescence emissions at room temperature in barium zirconate powders

L.S. Cavalcante^{a,b,*}, J.C. Sczancoski^b, J.W.M. Espinosa^{a,b}, V.R. Mastelaro^c, A. Michalowicz^d, P.S. Pizani^b, F.S. De Vicente^c, M.S. Li^c, J.A. Varela^a, E. Longo^a

^a Instituto de Química, UNESP, P.O. Box 355, 14801-907, SP, Araraquara, SP, Brazil

^b Departamento de Química e Física, UFSCar, P.O. Box 676, 13565-905, São Carlos, SP, Brazil

^c Instituto de Física de São Carlos, USP, P.O. Box 369, 13560-970, São Carlos, SP, Brazil

^d Université Paris XII, Faculté des Sciences et Technologie Bâtiment Marie Curie (P2)-345b, 94010, France

ARTICLE INFO

Article history:

Received 16 February 2008

Accepted 14 March 2008

Available online 5 May 2008

Keywords:

Disordered systems

Clusters

Chemical synthesis

Order–disorder effects

EXAFS

ABSTRACT

Intense blue and green photoluminescence (PL) emissions were observed at room temperature in barium zirconate (BaZrO_3) powders prepared by chemical method. The powders were analyzed by X-ray diffraction (XRD), X-ray absorption near edge spectroscopy (XANES), extended X-ray absorption spectroscopy (EXAFS) and ultraviolet–visible (UV–vis) absorption spectroscopy. The XRD patterns indicated the presence of a secondary phase of BaCO_3 in BaZrO_3 powders heat treated at 773 K. K-edge XANES data revealed that Zr atoms presents in at least two Zr environments. EXAFS investigations showed strong bond length dispersion in the first coordination shell around Zr atoms. EXAFS analysis indicated that Zr atoms are coordinated by 6 oxygen in BaZrO_3 powders heat treated at 973 K. UV–vis measurements suggested the presence of intermediary energy levels into the band gap of BaZrO_3 powders heat treated at 773 K. The intense PL emission in BaZrO_3 powders can be attributed to the two Zr environments or ZrO_5 – ZrO_6 clusters.

© 2008 Elsevier B.V. All rights reserved.

1. Introduction

Recently, several studies have been dedicated to the photoluminescence phenomenon, especially in BaTiO_3 perovskite, mainly due to their excellent optical properties [1–3]. In particular, the literature reports several theories on the wide band visible emission observed in crystalline titanates, which belongs to a universal “green-luminescence”. This characteristic property is practically observed for all self-activated ABO_3 perovskites titanates [4]. The origin of green luminescence has been explained and discussed in many papers by different mechanisms, including self-trapped excitons [5], recombination of electron and hole polarons, charge transfer vibronic exciton [6], donor–acceptor recombination [7], transitions in MeO_6 complexes [8] and structurally disordered titanates [9–11]. However, few investigations on this phenomenon in zirconates have been reported [12–16]. In particular, the literature reports some works on luminescence of crystalline BaZrO_3 doped with europium [17–19]. In general, BaZrO_3 presents interesting properties for application in electroceramics and refractories owing to their thermal resistance and conductivity [20]. This per-

ovskite can also be used as a protective agent against corrosion in the growth of superconductors [21,22]. Moreover, the excellent thermomechanical property [23] of this material is interesting for aerospace industries and correlated areas. This perovskite when doped can be used in fuel cells and proton conductors [24]. However, we have not knowledge about studies that explain the blue and green photoluminescence (PL) emissions in BaZrO_3 powders with intermediary structural order and/or structural order–disorder.

Therefore, in this paper we report on the intense blue and green PL emissions at room temperature in BaZrO_3 powders with structural order–disorder. The structural order–disorder in BaZrO_3 powders was analyzed by X-ray diffraction (XRD), X-ray absorption near edge spectroscopy (XANES) and extended X-ray absorption fine structure (EXAFS) spectroscopy techniques and ultraviolet–visible (UV–vis) absorption spectroscopy.

2. Experimental procedure

2.1. Synthesis of BaZrO_3 powders

BaZrO_3 powders were synthesized by the polymeric precursor method. Barium nitrate, $\text{Ba}(\text{NO}_3)_2$ (99.9% Aldrich), zirconium *n*-propoxide, $[\text{Zr}(\text{OC}_3\text{H}_7)_4]$ (99.9% Aldrich), ethylene glycol, $\text{C}_2\text{H}_6\text{O}_2$ (99.5% Synth) and citric acid, $\text{C}_6\text{H}_8\text{O}_7$ (99.5% Synth) were used as raw materials. Zirconium citrate was formed by the dissolution of $[\text{Zr}(\text{OC}_3\text{H}_7)_4]$ in a citric acid aqueous solution under constant stirring. The citrate solution was stirred at 358 K until to obtain a clear and homogeneous. $\text{Ba}(\text{NO}_3)_2$ was dissolved and added in a stoichiometric quantity to the Zr citrate solution. Ammo-

* Corresponding author at: Departamento de Química e Física, UFSCar, P.O. Box 676, 13565-905, Araraquara e São Carlos, SP, Brazil. Tel.: +55 16 3361 5215.

E-mail address: laecios@bol.com.br (L.S. Cavalcante).

nium hydroxide NH_4OH (30% NH_3 Synth) was added to adjust the pH ($\approx 7\text{--}8$) and to avoid the precipitation of barium citrate, which is favored in an acid solution [25]. After homogenization of the solution containing Ba^{2+} cations, $\text{C}_2\text{H}_6\text{O}_2$ was added to promote a polyesterification reaction [26]. The citric acid/ethylene glycol ratio in mass was fixed at 60/40. The resulting polymeric resin was then placed in a conventional furnace and heated treated at 623 K for 4 h with a heating rate fixed at 278 K/min to promote the pulverization and decomposition of the organic part from citric acid and ethylene glycol. The obtained precursor powders were annealed at 773 and 973 K for 2 h in a tube furnace with oxygen atmosphere, using a heating rate fixed at 274 K/min.

2.2. Characterizations of BaZrO_3 powders

The crystalline phase was analyzed by X-ray diffraction (XRD) patterns recorded on a (Rigaku-DMAX2500PC) with $\text{Cu K}\alpha$ radiation in the 2θ range from 10° to 75° with $0.02^\circ/\text{min}$. PL spectra in the range from 488 to 800 nm were taken with a U1000 Jobin-Yvon double monochromator coupled to a cooled GaAs photomultiplier and a conventional photon counting system. The 488.0 nm wavelength of an argon ion laser was used as excitation source, using a maximum output power kept at 30 mW. Cylindrical lens were used to prevent the sample from overheating. The slit width used was 100 μm . PL spectra in the range from 380 to 800 nm were measured with a Thermal Jarrel-Ash Monospec 27 monochromator and a Hamamatsu R446 photomultiplier. The 350.7 nm line of a krypton ion laser (Coherent Innova 90K) was used as excitation source, with the lasers nominal output power kept at 200 mW. X-ray absorption near-edge structure (XANES) and extended X-ray absorption fine structure (EXAFS) spectra of the BaZrO_3 powders were collected at the Zr K-edge using a Si (220) monochromator in the D04B-XAFS1 beam line. The powders were deposited on a polymeric membrane and the incident and transmitted X-ray beam were detected by ionization chambers filled with Ar gas. XANES spectra were measured from 50 eV below and 200 eV above the edge with energy step of 1.0 eV near the edge region. For comparison, all XANES spectra were background removed and normalized using as unity the 100 eV after the edge. The energy range of the Zr K-edge EXAFS spectra was 17,900–18,900 eV and it was calibrated using Zr foil. Data were collected at room temperature using energy steps of 2 eV and an integration time of 3 s. Three EXAFS spectra were collected for each sample and the average spectrum was used to perform the data analysis. The qualitative analysis of the EXAFS spectra was carried out by using the program set written by Michalowicz [27] according to the recommended procedures described in ref. [28]. Due to the low signal to noise ratio at high k values, the analysis of the EXAFS spectra were limited to the maximum value of 12 \AA^{-1} . After atomic absorption removal and normalization, the $k\chi(k)$ weighted EXAFS signal was Fourier transformed to R distance space in the $2.7\text{--}12.9 \text{ \AA}^{-1}$ range. Each spectrum was Fourier transformed using a Kaiser apodisation window with $\tau = 2.5$. The contribution of first coordination shell around zirconium atoms was extracted by a back Fourier transform in R distance space and then fitted using theoretical phase and amplitude functions as obtained from FEFF8.2 code [29]. Ultraviolet–visible (UV–vis) absorption spectra of optical absorbance on disordered and ordered BaZrO_3 powders were recorded using a Cary 5G spectrophotometer.

3. Results and discussion

3.1. X-ray diffraction analysis

The XRD patterns of BaZrO_3 powders heat treated at 773 and 973 K for 2 h in oxygen atmosphere are shown in Fig. 1.

The presence of diffraction peaks can be used to evaluate the structural order at long-range or periodicity of the material. BaZrO_3 phase was confirmed by comparison between the XRD patterns with the respective Joint Committee on Powder Diffraction Standards (JCPDS) card No. 06-0399. All diffraction peaks of BaZrO_3 powders heat treated at 973 K for 2 h were indexed as a cubic structure (see Fig. 1). However, BaZrO_3 powders heat treated at 773 K for 2 h showed diffraction peaks related to the BaZrO_3 cubic and also of barium carbonate (BaCO_3). Before complete structural organization, BaZrO_3 powders passes by an intermediary structural organization or structural order–disorder.

3.2. X-ray absorption near edge spectroscopy analysis

Fig. 2 shows the Zr K-edge XANES spectra of BaZrO_3 powders.

For the K-edge of Zr, the main absorption peak can be assigned to the $1s$ to $5p$ transitions [30]. As can be observed, XANES spectra of BaZrO_3 powders heat treated at 773 K present a significant

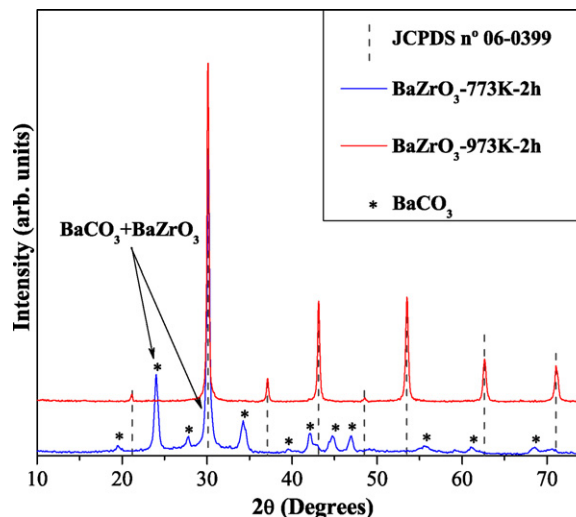


Fig. 1. XRD patterns of BaZrO_3 powders heat treated at 773 and 973 K for 2 h in oxygen atmosphere.

difference in the main absorption edge in relation to the spectra of the BaZrO_3 powders were noted with a double peak (see Fig. 2). The peak localized between 18,050 and 18,125 eV placed at a high energy in the XANES spectra for the BaZrO_3 powder heat treated at 973 K has been attributed to the multiple scattering due to the strong Zr–Zr and Zr–Ba correlations [31]. In BaZrO_3 powders crystallized at 973 K, the Zr atoms are first coordinated by 6 oxygen atoms situated at 2.09 Å . With regard to the main absorption edge feature of BaZrO_3 powders heat treated at 773 K, the XANES spectra are quite similar with those of zirconia silica xerogels [31]. In this work, the XANES spectra are characteristic of Zr atoms in at least two Zr environments. We attributed this behavior, based on our previous XANES results presented in the crystallization process for titanates: SrTiO_3 , PbTiO_3 and CaTiO_3 [32–34], which indicated the coexistence of two types of environments for the titanium, called of five-fold titanium coordination ($[\text{TiO}_5]$ square-base pyramid) and six-fold titanium coordination ($[\text{TiO}_6]$ octahedron). In this paper, we presume the existence of $[\text{ZrO}_6]$ – $[\text{ZrO}_5]$ clusters in the latticed of BaZrO_3 powders heat treated at 973 K for 2 h. In the lattice of BaZrO_3 powders heat treated at 773 K for 2 h, we believe that the presence of $[\text{ZrO}_6]$ – $[\text{ZrO}_5]$ clusters. Where $[\text{ZrO}_5]$ can be linked to neutral oxygen vacancies (V_O^\times), singly ionized ($\text{V}_\text{O}^\bullet$) and double ionized ($\text{V}_\text{O}^{\bullet\bullet}$). For facility the comprehension, we attribute the presence of struc-

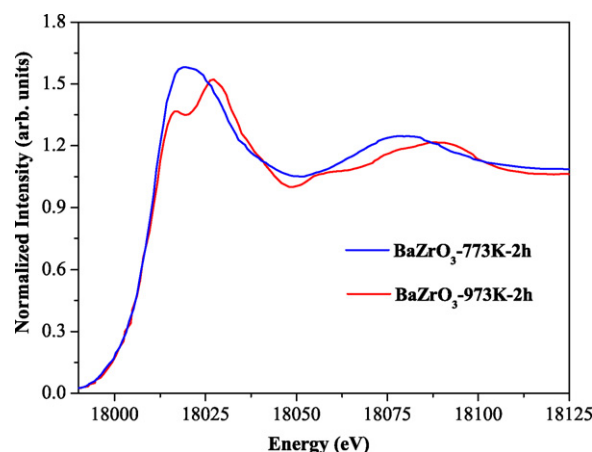


Fig. 2. XANES spectra of BaZrO_3 powders heat treated at 773 and 973 K for 2 h in oxygen atmosphere.

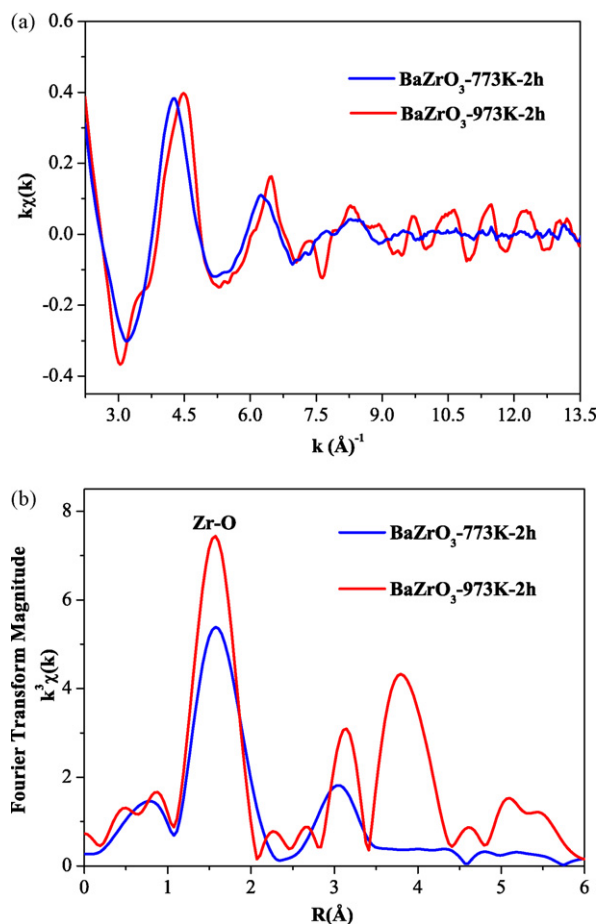


Fig. 3. (a) k weighted normalized EXAFS spectra of BaZrO_3 powders and (b) respective Fourier transform magnitude of the k^3 -weighted EXAFS spectra.

tural order-disorder for the BaZrO_3 powder heat treated at 773 K for 2 h.

In sequence to quantify the structural differences observed on the XANES spectra, we analyze the EXAFS spectra of BaZrO_3 powders heat treated at 773 and 973 K. In this work, the XANES spectra are characteristic of Zr atoms at least in two Zr environments. Usually, EXAFS spectra provide information on the coordination chemistry of the probe atom, including such as average bond lengths and coordination numbers.

3.3. Extended X-ray absorption spectroscopy analysis

Fig. 3(a) shows the $k\chi(k)$ EXAFS spectra of BaZrO_3 powders heat treated at 773 and 973 K and Fig. 3(b) their respective $k^3\chi(k)$ Fourier transform magnitude.

EXAFS spectrum of crystalline powders is quite similar to that reported in the literature [35]. As can be seen in Fig. 3(a), EXAFS spectrum of BaZrO_3 powders heat treated at 773 K is highly smooth at high k values, indicating that the structure is considerably disordered when compared to that the powders heat treated at 973 K. To obtain quantitative structural information on the Zr–O first coordination shell in both samples, the first peak of the Fourier transform magnitude presented in Fig. 3(b) was selected and again the Fourier transform was employed to obtain a filtered EXAFS spectrum related only to the first Zr–O coordination shell. The filtered EXAFS spectrum was then fitted using the theoretical phase and amplitude functions provided by the FEFF8.2 code [35].

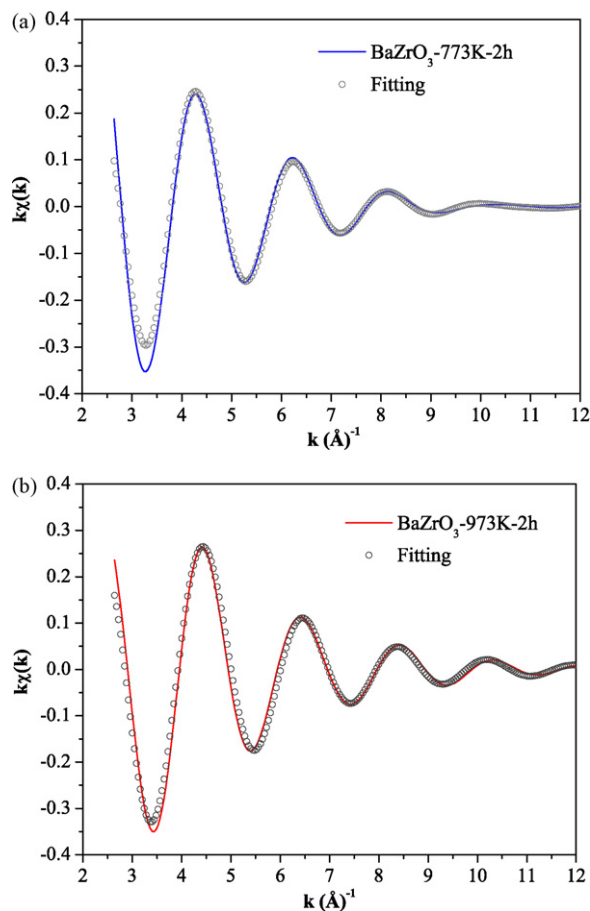


Fig. 4. Comparison between filtered experimental EXAFS data (solid line) and refined data (dots) of BaZrO_3 powders heat treated at (a) 773 K and (b) 973 K for 2 h in oxygen atmosphere.

Fig. 4(a) and (b) show the experimental and best fit of the filtered EXAFS spectra of both samples.

According to the fitting results presented in Table 1, the first coordination shell around Zr atoms in BaZrO_3 powders heat treated at 973 K is composed by 6 oxygen atoms situated at approximately 2.11 Å (see Fig. 4(b)).

These results are consistent with the XRD data of crystalline BaZrO_3 powders, $N_{\text{Zr-O}} = 6$, $R = 2.09$ Å [35]. On the other hand, in the case of BaZrO_3 powders heat treated at 773 K, which were characterized as being structurally ordered-disordered based on XRD data, the best fitting of the filtered EXAFS spectra was achieved with a structural model composed by 3 shells with a bond length in the range from 2.06 to 2.31 Å (see Table 1 and Fig. 4(a)). This strong bond length dispersion in the first coordination shell around Zr atoms for the BaZrO_3 powders heat treated at 773 K explains the significant difference observed in the intensity of the first peak of the Fourier transform localized between 1 and 2 Å (see Fig. 3(b)).

Table 1

Structural results obtained from the fitting of BaZrO_3 powders by the EXAFS spectra

T (K)	N	R (Å)	σ^2 (Å) ²	ΔE (eV)	QF
773	1.8 ± 0.5	2.06 ± 0.0008			
	2.8 ± 0.3	2.18 ± 0.0008	$0.000 \pm 0.002^*$	$2.3 \pm 0.8^*$	1.47
	1.3 ± 0.3	2.31 ± 0.0008			
973	5.8 ± 0.5	2.108 ± 0.0008	0.007 ± 0.002	2.0 ± 0.7	2.54

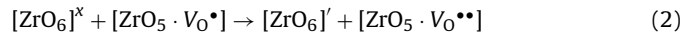
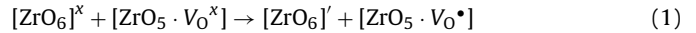
N is the first coordination shell neighbor number, σ is the Debye-Waller Factor, R is the Zr–O mean bond length, E is the threshold energy shift and QF is the quality factor [28].

3.4. BaZrO₃ structure and models

BaZrO₃ powders presented a cubic structure with a space group $Pm\bar{3}m$. The experimental lattice parameters values crystalline BaZrO₃ phase were $a = b = c = 4.186 \text{ \AA}$. These parameters were calculated using the least squares refinement of the UNITCELL-97 program [36]. The representation of an ordered BaZrO₃-o model was built through $1 \times 1 \times 2$ supercell (Fig. 5(a)) [37]. This ordered model can be designed as [ZrO₆]-[ZrO₆], since each Zr atom is surrounded by six O atoms. We assumed that before complete crystallization of BaZrO₃ powders, i.e., before heat treatment temperature reach to 973 K, the structure of this material was composed by a mixture of ZrO₆ octahedra surrounded by Ba atoms. The ordered-disordered BaZrO₃-od model was formed by the displacement of one Zr atom in the [001] direction. This displacement was the simplest way to represent the two environments of Zr to show the [ZrO₅ · V_O²] complex clusters, where V_O² = V_O^x, V_O[•] and V_O^{••} are designed as square-base pyramid, and [ZrO₆] designed as octahedron. Therefore, BaZrO₃-od structure can be represented by [ZrO₅ · VO²]-[ZrO₆], as shown in Fig. 5(b).

As can be seen in Fig. 5, this simple model suggests a mechanism for structural organization of BaZrO₃ powders prepared by the polymeric precursor method. After increase of heat treatment temperature occurs a reduction of oxygen vacancies in the BaZrO₃ lattice. This approach leads to a correlation between experimental data and model proposed. This slight order degree on structurally disordered materials was expected, since two or more atoms arranged near to each other on a stable configuration must necessarily have some order degree because of the existence of a minimum potential energy. Our purpose with the BaZrO₃-od model

is to provide a simple scheme to help in the comprehension of PL emission mechanisms linked to the structural defects of the electronic structure without to suppress completely the geometry of the cell. Using the same distorted model, we have successfully explained the PL emission of several titanates [38–40] and zirconates titanates [41–43]. The model suggests that the increase of heat treatment temperature reduces the disorder in BaZrO₃ lattice, creating electron-captured oxygen vacancies. According to the equations using the Kröger-Vink notation by means of complex clusters [44a,b].



where [ZrO₆]' is a donor, [ZrO₅ · V_O[•]] is a donor-acceptor, and [ZrO₅ · V_O^{••}] is an acceptor.

3.5. Ultraviolet-visible absorption spectroscopy analysis

Fig. 6 shows UV-vis absorption spectra of BaZrO₃ powders heat treated at 773 and 973 K for 2 h in oxygen atmosphere.

The exponential optical absorption edge and optical band gap are controlled by the structural order-disorder degree in the BaZrO₃ lattice. The increase in the band gap can be associated to the reduction of defects in the lattice, which decrease the intermediary energy levels into the band gap region of disordered BaZrO₃ powders. The powders heat treated at 773 K presented a similar absorption behavior as in amorphous semiconductors, such as silicon and insulators (see Fig. 6(a)). Therefore, BaZrO₃ powders heat

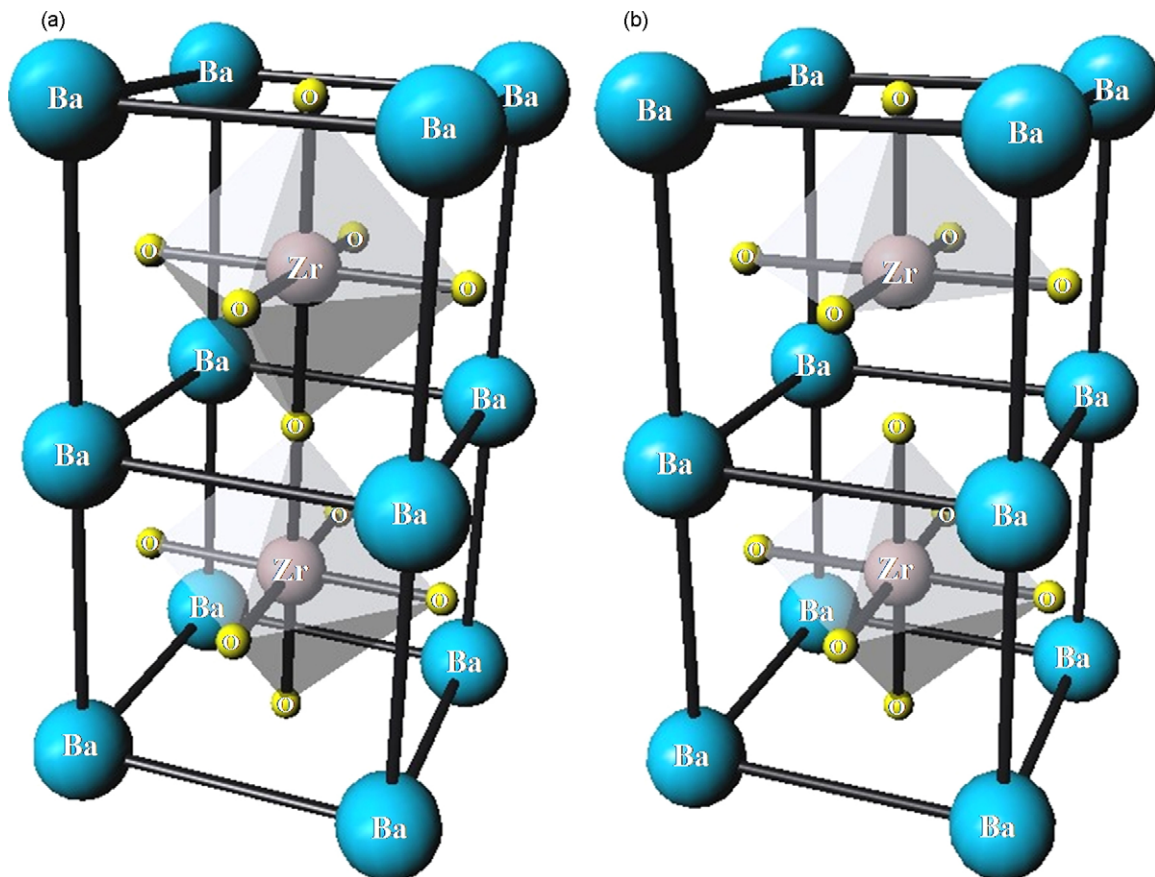


Fig. 5. Supercell representation $1 \times 1 \times 2$ of BaZrO₃ cubic structure: (a) ordered BaZrO₃-o model and (b) ordered-disordered BaZrO₃-od model.

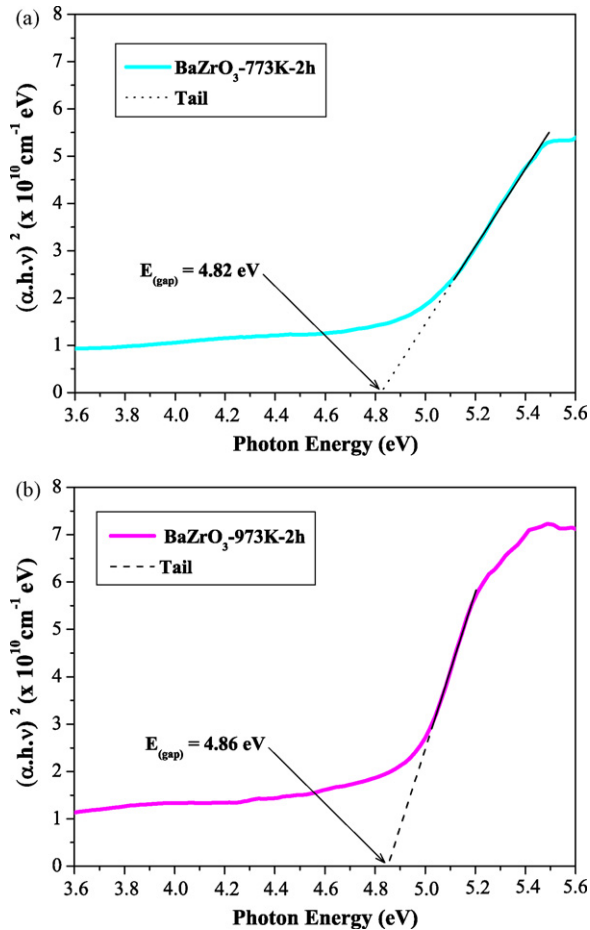


Fig. 6. UV-vis absorbance spectra of BaZrO₃ powders heat treated at (a) 773 K and (b) 973 K for 2 h in oxygen atmosphere.

treated at 973 K showed a typical band in the high energy region of the absorbance curve for ordered or crystalline materials (see Fig. 6(b)). In disordered BaZrO₃ powders, the absorbance measurements suggest a non-uniform on band gap structure with the presence of localized states. The optical band gap energy is related to the absorbance and photon energy, according to Wood and Tauc [45] as shown in Eq. (4):

$$h\nu \propto (h\nu - E_g^{\text{opt}})^2, \quad (4)$$

where α is the absorbance, h is the Planck constant, ν is the frequency, and E_g^{opt} is the optical band gap.

In this case, optical band gap was determined extrapolating the linear portion of the curve or tail. The obtained result for the BaZrO₃ heat treated at 773 K for 2 h was of 4.82 eV and 4.86 eV for BaZrO₃ crystalline. This observed behavior can be associated with the energy difference between the valence band and conduction band for this material.

3.6. Wide band model and photoluminescence analysis

Fig. 7 illustrates the wide band model and PL spectra recorded at room temperature for the BaZrO₃ powders heat treated at 773 and 973 K for 2 h using two different excitation wavelengths: 350.7 and 488 nm.

Fig. 7(a) shows the lasers employed in the excitation of BaZrO₃ powders heat treated annealed at 773 and 973 K for 2 h. Depending upon the excitation wavelengths used is possible to promote electrons from the valence band to conduction band. The optical band gap for the BaZrO₃ powders heat treated at 773 K and 973 K were 4.82 eV and 4.86 eV, respectively. In this case, it was not verified an emission by band-band process, but due to the wide band process. Our wide band model presented in Fig. 7(b), before the absorption of $h\nu$, can occur by two possible mechanisms: shallow holes (see Fig. 7(c), above) and deep holes (see Fig. 7(c), below). These mechanisms are responsible by different light emissions in disordered BaZrO₃ powders. This phenomena was not observed on structurally ordered powders, possibly due to the simultaneous

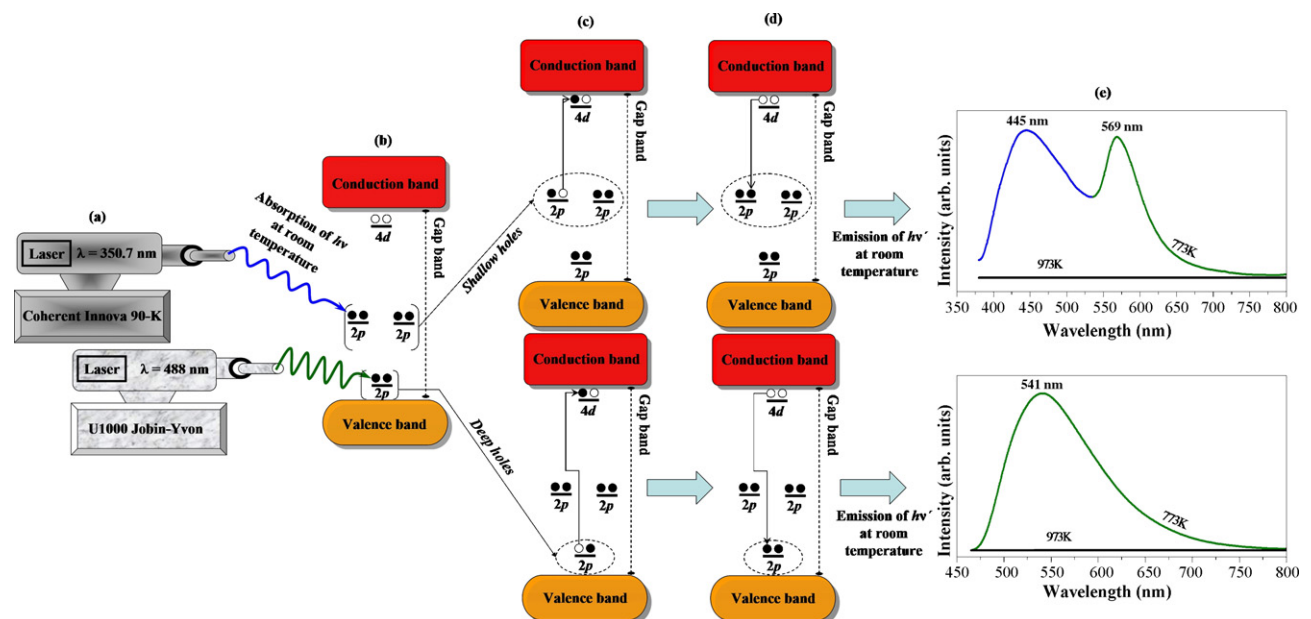


Fig. 7. (a) Lasers employed in the excitation process of BaZrO₃ powders, (b) wide band model, before excitation, (c) excitation-formation of self-trapped excitons (STEs): above = shallow holes and below = deep holes, (d) after excitation-recombination of e^- and h^+ for formation of PL blue and/or green emission and (e) PL spectra of BaZrO₃ powders heat treated at 773 and 973 K for 2 h in oxygen atmosphere.

presence of $[\text{ZrO}_6]-[\text{ZrO}_6]$ in the lattice. This behavior is agreement with XANES and EXAFS results and with the models described previously in this manuscript. Fig. 7(d) shows the excitation process due to the recombination between electrons (e') and holes (h^*) into band gap, which are responsible by the blue and/or green PL emission at room temperature.

The general aspect of the spectra is a broad band covering a large part of the visible spectra from 400 to 800 nm. A set of emission bands is distinctly recorded under the two wavelengths, with the peak position of each band shifts upward when the excitation wavelength increases. These two distinct energies (~ 3.54 and 2.54 eV) are able to excite different populations of electrons localized in additional levels in the forbidden band gap of disordered BaZrO_3 powders. The PL emission profile is typical of a multiphonon and multilevel process, i.e., a system in which relaxation occurs by several paths, involving the participation of numerous states into the band gap of the material. This behavior is related to the structural disorder of BaZrO_3 and confirms the presence of additional electronic levels in the forbidden band gap. Therefore, many of the oxygen vacancies are vacancy complexes on the intermediate structure. In this cubic structure, $[\text{ZrO}_5 \cdot \text{V}_\text{O}^\bullet]$ complex cluster is a donor candidate and $[\text{ZrO}_6]^\times$ an acceptor candidate. We speculated that these oxygen complex vacancies induce new energy levels in the band gap, which can be attributed to the zirconium–oxygen complex vacancy centers.

The blue emission can be attributed to shallow holes in the band gap of materials with a structural order–disorder. The green emissions are linked to deep holes into the band gap for more disordered materials. The PL emission can be attributed to the presence of the structural order–disorder degree in the lattice due to the presence of $[\text{ZrO}_5 \cdot \text{V}_\text{O}^\bullet]$ and $[\text{ZrO}_5 \cdot \text{V}_\text{O}^{\bullet\bullet}]$ complex clusters deeply inserted in the band gap. The increase of the structural order leads to a reduction of complex vacancies and consequently the PL emission disappear. The intensity of PL emission depends mainly on the interaction of these complex clusters and of the excitation wavelength. Time-resolved spectroscopy is necessary to confirm this statement, which has already been investigated by several papers [46–49].

4. Conclusions

BaZrO_3 powders prepared by a chemical method were characterized by XRD, XANES, EXAFS and UV–vis techniques. XANES and EXAFS investigations suggested that the defects in the BaZrO_3 lattice can be linked to the two environments Zr correlated with the $[\text{ZrO}_5 \cdot \text{V}_\text{O}^\bullet]-[\text{ZrO}_6]$ complex clusters, indicating a possible oxygen deficiency in BaZrO_3 powders with structural ordered–disordered. The results also indicated that the structural evolution from order–disorder to order is due to the increase of heat treatment temperature, which promote a reduction of local disorder and favors the increase of band gap. BaZrO_3 powders obtained by the chemical method heat treat at 773 K presented an intense PL emission at room temperature around 541 nm when excited by 488 nm wavelengths and around 445 and 569 nm when excited by 350.7 nm wavelengths. Also it was observed that the use of wavelengths with energy close to the band gap value of the material are able to activate some energy levels into the band gap. We attributed the shallow holes with blue PL emission and the deep holes with a green PL emission in disordered BaZrO_3 powders.

Acknowledgements

The authors thank the financial support of the Brazilian research financing institutions: CAPES, FAPESP, CNPq and to Laboratório Nacional de Luz Síncrotron (LNLS).

References

- [1] J.F. Meng, Y. Huang, W.F. Zhang, Z. Du, Z. Zhu, G. Zou, *Phys. Lett. A* 2005 (1995) 72.
- [2] R.I. Eglitis, V.A. Trepakov, S.E. Kapphan, G. Borstel, *Solid State Commun.* 126 (2003) 301.
- [3] F.M. Pontes, C.D. Pinheiro, E. Longo, E.R. Leite, S.R. de Lazaro, R. Magnani, P.S. Pizani, T.M. Boschi, F. Lanciotti, *J. Lumin.* 104 (2003) 175.
- [4] L. Jastrabik, S.E. Kapphan, V.A. Trepakov, I.B. Kudyk, R. Pankrath, *J. Lumin.* 102 (2003) 657.
- [5] M. Aguilar, F. Agulló-López, *J. Appl. Phys.* 53 (1982) 9009.
- [6] V.S. Vikhniin, R.I. Eglitis, S.E. Kapphan, E.A. Kotomin, G. Borstel, *Eur. Phys. Lett.* 56 (2001) 702.
- [7] E. Yamaichi, K. Watanabe, K. Ohi, *J. Phys. Soc. Jpn.* 57 (1988) 2201.
- [8] G. Blasse, *Mater. Res. Bull.* 18 (1983) 525.
- [9] P.S. Pizani, E.R. Leite, F.M. Pontes, E.C. Paris, J.H. Rangel, E.J.H. Lee, E. Longo, P. Delega, J.A. Varela, *Appl. Phys. Lett.* 77 (2000) 824.
- [10] E.R. Leite, L.P.S. Santos, N.L.V. Carrenó, E. Longo, C.A. Paskocimas, J.A. Varela, F. Lanciotti, C.E.M. Campos, P.S. Pizani Jr., *Appl. Phys. Lett.* 78 (2001) 2148.
- [11] P.S. Pizani, H.C. Basso, F. Lanciotti, T.M. Boschi, F.M. Pontes, E. Longo, E.R. Leite Jr., *Appl. Phys. Lett.* 81 (2002) 253.
- [12] A. Zhang, M. Lü, S. Wang, G. Zhou, S. Wang, Y. Zhou, *J. Alloys Compd.* 433 (2007) L7.
- [13] G.F.G. Freitas, R.S. Nasar, M. Cerqueira, D.M.A. Melo, E. Longo, P.S. Pizani, J.A. Varela, *Ceram. Int.* 29 (2003) 793.
- [14] G. Blasse, G. Bernardi, D.J.W. Ijdo, J.R. Plaisier, *J. Alloys Compd.* 217 (1995) 29.
- [15] V.M. Longo, L.S. Cavalcante, A.T. de Figueiredo, L.P.S. Santos, E. Longo, J.A. Varela, C.A. Paskocimas, F.S. De Vicente, A.C. Hernandez, *Appl. Phys. Lett.* 90 (2007) 091906.
- [16] M.M. Gentleman, D.R. Clarke, *Surf. Coat. Technol.* 200 (2005) 1264.
- [17] X.H. Liu, X.D. Wang, *Opt. Mater.* 30 (2007) 626.
- [18] Z. Lu, Y. Tang, L. Chen, Y. Li, *J. Cryst. Growth* 266 (2004) 539.
- [19] H. Zhou, Y. Mao, S.S. Wong, *J. Mater. Chem.* 17 (2007) 1707.
- [20] S. Yamanaka, T. Hamaguchi, T. Oyama, T. Matsuda, S.-I. Kobayashi, K. Kurosaki, *J. Alloys Compd.* 359 (2003) 1.
- [21] A. Erb, E. Walker, R. Flükiger, *Physica C* 245 (1995) 245.
- [22] R. Liang, D.A. Bonn, W.N. Hardy, *Physica C* 304 (1998) 105.
- [23] K.C. Goretta, E.T. Park, R.E. Koritala, M.M. Cuber, E.A. Pascual, N. Chen, A.R. de Arellano-Lopez, J.L. Routbort, *Physica C* 309 (1998) 245.
- [24] S. Tao, J.T.S. Irvine, *J. Solid State Chem.* 180 (2007) 3493.
- [25] J. Tsay, T. Fang, *J. Am. Ceram. Soc.* 82 (1999) 1409.
- [26] T. Salmi, E. Paatero, P. Nyholm, *Chem. Eng. Proc.* 43 (2004) 1487.
- [27] A. Michalowicz, *J. Phys. IV* 7 (1997) 235.
- [28] S.S. Hasnain (Ed.), Report on the International Workshops on Standards and Criteria in XAFS, in: *X-ray Absorption Fine Structure: Proceedings of the VI International Conference on X-ray Absorption Fine Structures*. Ellis Horwood, New York, p. 752, 1991.
- [29] A.L. Ankudinov, B. Ravel, J.J. Rehr, S.D. Conradson, *Phys. Rev. B* 58 (1998) 7565.
- [30] C.M. Wang, G.S. Cargill, H.M. Chan, M.P. Harmer, *J. Am. Ceram. Soc.* 85 (2002) 2492.
- [31] G. Mountjoy, D.M. Pickup, R. Anderson, G.W. Wallidge, M.A. Holland, N.J. Newport, M.E. Smith, *Phys. Chem. Phys.* 2 (2000) 2455.
- [32] F.M. Pontes, E. Longo, E.R. Leite, E.J.H. Lee, J.A. Varela, P.S. Pizani, C.E.M. Campos, F. Lanciotti, C.D. Pinheiro, *Mater. Chem. Phys.* 77 (2003) 598.
- [33] E.R. Leite, E.C. Paris, F.M. Pontes, C.A. Paskocimas, E. Longo, F. Sensato, C.D. Pinheiro, J.A. Varela, P.S. Pizani, C.E.M. Campos, F. Lanciotti Jr., *J. Mater. Sci.* 38 (2003) 1175.
- [34] S. de Lazaro, J. Milanez, A.T. de Figueiredo, V.M. Longo, V.R. Mastelaro, F.S. De Vicente, A.C. Hernandez, J.A. Varela, E. Longo, *Appl. Phys. Lett.* 90 (2007) 111904.
- [35] Y. Zhao, D.J. Weidner, *J. Phys. Chem. Miner.* 18 (1991) 294.
- [36] T.J.B. Holland, S.A.T. Redfern, *Miner. Mag.* 61 (1997) 65.
- [37] <http://www.jcrystal.com/steffenweber/JAVA/JSV/jsv.html>.
- [38] M.F.C. Gurgel, J.W.M. Espinosa, A.B. Campos, I.L.V. Rosa, M.R. Joya, A.G. Souza, M.A. Zaghete, P.S. Pizani, E.R. Leite, J.A. Varela, E. Longo, *J. Lumin.* 126 (2007) 771.
- [39] I.A. Souza, M.F.C. Gurgel, L.P.S. Santos, M.S. Góes, S. Cava, M. Cilense, I.L.V. Rosa, C.O. Paiva-Santos, E. Longo, *Chem. Phys.* 322 (2006) 343.
- [40] E. Orhan, F.M. Pontes, C.D. Pinheiro, E. Longo, P.S. Pizani, J.A. Varela, E.R. Leite, T.M. Boschi, A. Beltrán, J. Andrés, *J. Eur. Cer. Soc.* 25 (2005) 2337.
- [41] E. Orhan, F.M. Pontes, C.D. Pinheiro, T.M. Boschi, E.R. Leite, P.S. Pizani, A. Beltrán, J. Andrés, J.A. Varela, E. Longo, *J. Solid State Chem.* 177 (2004) 3879.
- [42] L.S. Cavalcante, M.F.C. Gurgel, A.Z. Simões, E. Longo, J.A. Varela, M.R. Joya, P.S. Pizani, *Appl. Phys. Lett.* 90 (2007) 011901.
- [43] M. Anicete-Santos, M.S. Silva, E. Orhan, M.S. Góes, M.A. Zaghete, C.O. Paiva-Santos, P.S. Pizani, M. Cilense, J.A. Varela, E. Longo, *J. Lumin.* 127 (2007) 689.
- [44] (a) F.A. Kröger, H.J. Vink, in: F. Seitz, D. Turnbull (Eds.), *Solid State Physics*, 3rd ed., Academic Press, New York, 1956, p. 307; (b) L.S. Cavalcante, M.F.C. Gurgel, E.C. Paris, A.Z. Simões, M.R. Joya, J.A. Varela, P.S. Pizani, E. Longo, *Acta Mater.* 55 (2007) 6416.
- [45] D.L. Wood, J. Tauc, *Phys. Rev. B* 5 (1972) 3144.
- [46] R. Leonelli, J.L. Brebner, *Solid State Commun* 54 (1985) 505.
- [47] R. Leonelli, J.L. Brebner, *Phys. Rev. B* 33 (1986) 8649.
- [48] R.I. Eglitis, E.A. Kotomin, G. Borstel, *Eur. Phys. J. B* 27 (2002) 483.
- [49] R.I. Eglitis, E.A. Kotomin, G. Borstel, *J. Phys.: Condens. Matter* 14 (2002) 3735.